1

Nanomaterials: Solar Energy Conversion

L.G. Paterno

INSTITUTE OF CHEMISTRY, DARCY RIBEIRO CAMPUS, UNIVERSITY OF BRASILIA, BRASILIA, BRAZIL

CHAPTER OUTLINE

1.1 Introduction

The increase in population density and economic growth in many parts of the world since 1980 has maintained a strong pace because of the availability of 15 terawatts (TW) of energy—our current consumption—at accessible prices. However, even the most optimistic forecasts cannot ensure that this scenario will persist in the coming decades. A large part of the world's energy consumption depends on fossil fuels, especially oil. However, extraction of "cheap oil" may reach its peak in the next few years and then decline. Therefore, production of energy from alternative sources is indispensable to maintain sustainable global economic growth and the perspective of the consumption of an additional 15 TW after 2050 [1]. We must also note in this new planning effort that the alternative sources of energy production must be clean, as gas emissions from fossil fuels have negatively contributed to the quality of life on the planet because of global temperature increases and air pollution [2].

In view of the imminent collapse of the current energy production system, it is necessary to seek alternative sources of energy production. Within the current scenario of scientific and technological development and the urgent demand for 30 TW by 2050 [1], there are at

Nanoscience and its Applications

least three alternative options for energy production [3]: (1) burning of fossil fuel associated with CO_2 sequestration, (2) nuclear energy, and (3) renewable energy. In option (1), emissions of greenhouse gases (GHGs), especially CO_2, can already be controlled by emission certificates known as carbon credits [4]. One ton of CO_2 is equal to one carbon credit. In practical terms, the Kyoto Protocol of 1999 establishes the maximum level of GHGs that a certain country can emit from its industrial activities. If a certain industry or country does not reach the established goals, it becomes a buyer of carbon credits equivalent to the excess emissions. By contrast, countries whose emissions are lower than the preestablished limit can sell their "excess" credits on the international market. However, this initiative is still controversial, mainly because, to many, it implies a discount on the penalty from the excessive emission of GHGs. Option (2) is very attractive because it is a clean type of energy, with high production efficiency and zero GHG emission [5]. Many European countries, as well as the United States and Japan, produce and consume electricity from nuclear plants [6]. However, the risk of accidents is constant, especially after the catastrophic events of Chernobyl (1986) [7] and Fukushima (2011) [8], and the improper use of nuclear technology for nonpeaceful purposes raises concerns. Energy production from renewable sources (3) is undoubtedly the most promising alternative [9]. The different technologies in this group, such as solar, wind, hydroelectric, and geothermal, are absolutely clean in terms of GHG emissions. Theoretically, energy production from the burning of biomass, such as wood, ethanol, and biodiesel, creates no net CO_2 emission because it is a closed cycle (the amount of CO_2 sequestered from the atmosphere during photosynthesis and transformed into biomass is the same amount released to the atmosphere when the biomass is combusted with O_2). In practical terms, the balance is slightly negative because land management, transportation, and processing use noncounterbalanced sources. Still, this balance is much less negative than the one associated with the burning of fossil fuels.

The conversion of solar energy into electricity is one of the most promising ways to produce clean and cheap energy from a renewable source [3,9,10]. Silicon-based solar cells, already manufactured in the 1950s for military and space applications, have been available for civilian use for at least three decades, mainly in buildings and for power generation at remote locations. The cost is decreasing with the increasing production scale and the corresponding reduction of the price of silicon [11]. In addition, research in the field of solar cells increased in the 1990s as a result of discoveries in the area of nanotechnology. Today, third-generation devices are being developed that use nanomaterials to convert solar light into electricity at significantly lower costs than those of conventional silicon cells [3]. Third-generation solar cells, such as organic solar cells (OSCs) and dye-sensitized solar cells (DSSCs or dye cells), are a reality, are being produced at pilot scale by small companies, and will be commercially available in the near future [12,13]. Nanotechnology research has also enabled the development of photoelectrochemical cells for artificial photosynthesis, whose efficiency is still low, but with a high potential to increase to levels that would make the cells commercially interesting [14]. The use of nanomaterials is decisive to fully achieve energy conversion in these new devices. In addition, the use of nanomaterials reduces the cost and the environmental impact of cell production to make such devices even more promising.

Initially, this chapter will present the principles of solar conversion and the operation of solar cells, with a focus on OSCs and DSSCs. Then, the role of nanomaterials in the different parts of each device and in their operation is discussed. The most recent data (until 2012) on the conversion performance of third-generation cells are provided. The last topic consists of a brief description of photoelectrochemical cells to produce solar fuels, considering that this subject is correlated to the previous ones. However, it is not the intention of this chapter to present a thorough literature review on this last subject, and the reader is encouraged to consult the references listed at the end of the chapter.

1.2 Conversion of Solar Energy Into Electricity

1.2.1 Solar Spectrum and Photovoltaic Performance Parameters

The Sun is the most abundant and sustainable source of energy available on the planet. The Earth receives close to 120,000 TW of energy from the Sun every year, an amount 10^4 larger than the current global demand [14]. The photons that reach the Earth as solar light are distributed across different wavelengths and depend on variables, such as latitude, time of day, and atmospheric conditions. This distribution, known as the solar spectrum, is shown in Fig. 1.1 [15].

The spectrum shows the solar incidence power per area per wavelength ($W\,m^{-2}\,nm^{-1}$), also known as irradiance, considering a bandwidth of 1 nm ($\Delta\lambda$) [16]. The terms AM0, AM1.0, and AM1.5 refer to solar spectra calculated according to different ASTM standards, appropriate for each type of application [17]. For example, spectra AM1.0 and AM1.5 are calculated according to standard ASTM G173 and are used as reference standards for terrestrial applications, whereas spectrum AM0, based on standard ASTM E 490, is used in

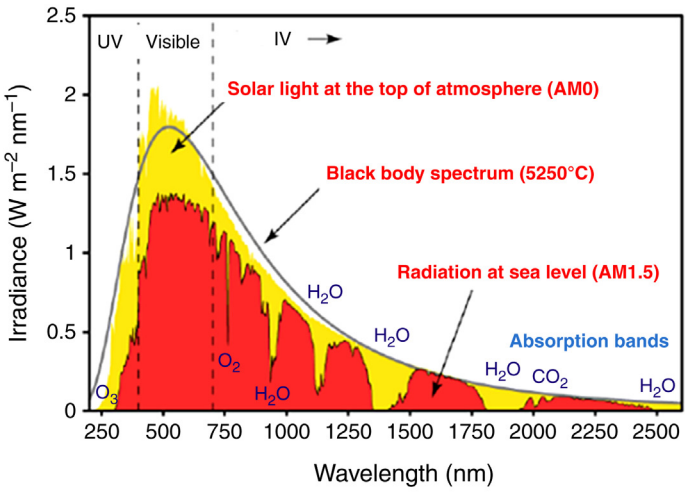

FIGURE 1.1 Solar spectrum expressed in W m^{-2} nm^{-1} according to AM0 and AM1.5 standards. *Adapted from http://org.ntnu.no/solarcells [15].*

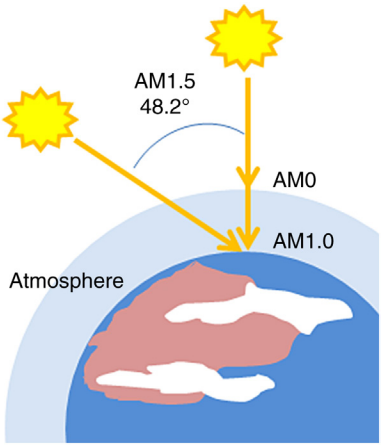

FIGURE 1.2 Schematics of the different forms of solar radiation incident on the Earth and the respective standards to calculate the solar spectrum. *Adapted from http://org.ntnu.no/solarcells [15].*

satellites. As shown schematically in Fig. 1.2, the calculation of the spectra considers specific geographic and atmospheric variables (i.e., the angle of incidence on the planet, the air density, and other parameters). The reproduction of the solar spectrum in the laboratory, according to the established standards, is fundamental to developing photovoltaic cells because it allows for comparison and certification of the performances of devices developed by different manufacturers and those still in development.

The performance of an illuminated solar cell is assessed by photovoltaic parameters, such as the power produced per illuminated cell area (P_{out}, in W·cm^{-2}), open-circuit voltage (V_{oc}, in V), short-circuit current density (J_{sc}, in mA·cm^{-2}), fill factor (*FF*), and overall conversion efficiency (η) [16]. All these parameters depend initially on the power of the light incident on the cell (P_{in}), given by Eq. 1.1 [16]:

$$P_{in} = \int_{\lambda} \frac{hc}{\lambda} \Phi_0(\lambda) d\lambda \tag{1.1}$$

where h is the Planck constant (4.14×10^{-15} eV·s), c is the speed of light (3.0×10^{8} m·s^{-1}), $\Phi(\lambda)$ is the flux of photons corrected for reflection and absorption before impacting the cell (cm^{-2} s^{-1} per $\Delta\lambda$), and λ is the wavelength of the incident light.

The open-circuit voltage corresponds to the voltage between the terminals (electrodes) of the illuminated cell when the terminals are open (infinite resistance). The short-circuit current density corresponds to the condition in which the cell's terminals are connected to a zero-resistance load. The short-circuit current density grows with the intensity of the incident light because the number of photons (and thus the number of electrons) also increases with intensity. Since the current usually increases with the active area of the solar cell, the current is conventionally expressed in terms of current density, J (current/area).

When a load is connected to a solar cell, the current decreases and a voltage is developed when the electrodes are charged. The resultant current can be interpreted as a

superposition of the short-circuit current caused by the absorption of photons and a dark current caused by the voltage generated by the load that flows in the opposite direction. Considering that solar cells usually consist of a p–n (p–n junction: junction of p-type and n-type semiconductors) or D–A [D–A junction: junction of an electron donor material (D) and an electron acceptor material (A)] junction, they can be treated as diodes. For an ideal diode, the dark current density (J_{dark}) is given by [16]

$$J_{dark}(V) = J_0(e^{qV/k_BT} - 1) \tag{1.2}$$

where J_0 is the current density at 0 K, q is the electron charge (1.6×10^{-19} C), V is the voltage between the electrodes of the cell, k_B is the Boltzmann constant (8.7×10^{-5} eV·K^{-1}), and T is the absolute temperature. The resultant current can be explained as a superposition of the short-circuit current and the dark current [16]:

$$J = J_{sc} - J_0(e^{qV/k_BT} - 1) \tag{1.3}$$

The open-circuit voltage is defined at $J = 0$, which means that the currents cancel and no current flows through the cell, which is the open-circuit condition. The resultant expression is given by [16]:

$$V_{oc} = \frac{k_BT}{q}\ln\left(\frac{J_{sc}}{J_0} + 1\right) \tag{1.4}$$

The performance parameters of a solar cell are determined experimentally from a current–voltage curve ($J \times V$), schematically represented in Fig. 1.3, when the cell is subjected to standard operating conditions, in other words, illumination according to standard AM1.5, under an irradiating flux of 100 W·cm^{-2} and a temperature of 25°C.

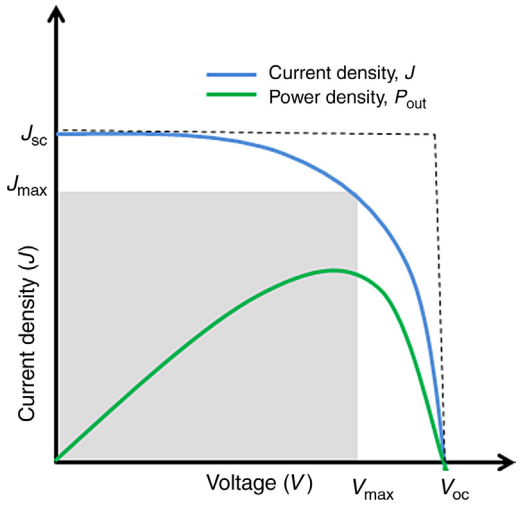

FIGURE 1.3 Current density–voltage ($J \times V$) curve of an illuminated solar cell.

The power density produced by the cell (P_{out}) (Fig. 1.3, gray area) is given by the product of the current density (J, in mA·cm^{-2}) and the corresponding operating voltage (V, in V) as per Eq. 1.5 [16]:

$$P_{out} = JV \tag{1.5}$$

The maximum power density (P_{max}) is given by

$$P_{max} = J_{max}V_{max} \tag{1.6}$$

Based on Fig. 1.3, it can be concluded that the maximum power produced by an illuminated solar cell is between $V = 0$ (short circuit) and $V = V_{oc}$ (open circuit), or V_{max}. The corresponding current density is given by J_{max}. The conversion efficiency of the cell (η) is given by the ratio between the maximum power and the incident power [16]:

$$\eta = \frac{J_{max}V_{max}}{P_{in}} \tag{1.7}$$

The behavior of an ideal solar cell may be represented by a $J \times V$ curve of rectangular shape (represented in the graph by dashed lines) where the current density produced is maximum, constant, and equal to J_{sc} up to the V_{oc} value. However, not all of the incident power is converted into energy by the cell, so in actual situations the $J \times V$ curve deviates from the ideal rectangular shape. The fill factor term (FF) is introduced to measure how close to the ideal behavior a photovoltaic cell operates. The FF is given by [16]

$$FF = \frac{J_m V_m}{J_{sc}V_{oc}} \tag{1.8}$$

By definition, $FF \leq 1$. Thus, the overall conversion efficiency can be expressed using the FF value [16]:

$$\eta = \frac{J_{sc}V_{oc}FF}{P_{in}} \tag{1.9}$$

In addition to these, another important performance parameter is the quantum efficiency, which measures how many electrons capable of performing work are generated by each incident photon of wavelength λ. The quantum efficiency is subdivided into internal and external classifications. The external quantum efficiency (EQE) measures the number of electrons collected by the electrode of the cell in the short-circuit condition divided by the number of incident photons. Also known as the incident photon to current efficiency (IPCE), its value is determined by Eq. 1.10 [16]:

$$\text{IPCE} = \frac{1240\, I_{sc}}{\lambda P_{in}} \tag{1.10}$$

Since the IPCE value depends on the wavelength of the incident radiation, an IPCE versus wavelength curve corresponds to the cell's spectral response, also known as the action

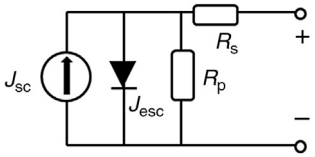

FIGURE 1.4 Equivalent circuit of a solar cell.

spectrum of the solar cell. The internal quantum efficiency (IQE) is the ratio of the number of electrons collected by the electrode of the cell in a short-circuit configuration divided by the number of photons that effectively enter the cell. This parameter does not consider all the incident photons because a portion of them is lost by reflection or absorption before they accomplish the charge separation process within the absorption layer. Both efficiencies are positive and ≤100%.

As already discussed, a solar cell can be understood as a power generator and can be represented by an equivalent circuit as in Fig. 1.4. The circuit has a solar cell, represented by the diode and its respective dark and short-circuit currents, and two resistances, one in series (R_s) and the other in parallel (R_p). The resistance in series represents the nonideal conductor behavior of the cell, whereas the resistance in parallel accounts for the leakage current inherent to any device, usually associated with insulation problems. In an ideal solar cell, $R_s = 0$, $R_p = \infty$, and the current expression initially represented by Eq. 1.3 can be expanded by including the resistances of the equivalent circuit, according to Eq. 1.11 [16]:

$$J = J_{sc} - J_0[e^{q(V+JAR_s/k_BT)} - 1] - \frac{V + JAR_s}{R_p} \tag{1.11}$$

where A is the active area of the cell in centimeter square.

1.2.2 Operating Principles of a Solar Cell

A typical solar cell consists of an absorbing material between two electrodes. The absorbing material can be either a semiconductor or a dye, organic, or inorganic, and it can be monocrystalline, polycrystalline, nanocrystalline, or amorphous [16]. The absorber collects (absorbs) the solar light and therefore must have a band separation energy (E_g) that matches the solar spectrum. The separation of charges into individual carriers and their transport may or may not be performed by the absorber. The electrodes are fabricated from conductive materials with different work functions, and one of them must be transparent to the incident light.

The photovoltaic conversion process can be divided into four sequential stages [16]:

1. light absorption causes an electron transition in the cell's absorbing material from the ground state to the excited state;
2. the excited state is converted into a pair of separate charge carriers, one negative and the other positive;

3. under an appropriate transport mechanism, the carriers move separately to the cell's electrical contacts; the negative carrier to the cathode and the positive carrier to the anode;
4. the electrons travel the circuit external to the cell, where they lose energy and perform useful work (i.e., to power a lamp or an engine). Then, they reach the cathode, where they recombine with the positive charge carriers and return the absorbing material to the ground state.

The mechanisms of (1) light absorption and (2) charge separation depend on the absorber's electron structure and morphology. In conventional solar cells made of inorganic semiconductors, such as silicon or gallium arsenide (GaAs) in the mono-, poly, and microcrystalline forms, absorption and separation are performed only by the absorber. The band separation energy of these semiconductors (Si: 1.1 eV; GaAs: 1.42 eV) is sufficient to collect close to 70% of the solar radiation incident on the planet. The absorbed photons promote the electrons to the conduction band and at the same time produce an equivalent number of gaps in the valence band of the absorbing material. The effect is observed both in direct-gap semiconductors, such as GaAs, and in indirect-gap semiconductors, such as Si [16]. Once formed, the charge carriers are separated in the semiconductor's junction region, which is formed at the interface of the p- and n-type doping regions (p–n junction), even when they are insulated by a third i-insulating region (p–i–n junction). The junction is obtained in the production of the absorbing film; a thin semiconductor film with a certain doping undergoes a second doping process, limited to a small depth. Thus, the final film has two different doping regions separated by an interface or junction. A built-in potential is created at the junction region because of the difference in electron affinities in each region. This potential is strong enough to separate the carriers into individual species, electron, and gap.

To better understand the operation of this type of device, Fig. 1.5 presents a schematic of the energy levels of p and n semiconductors, before and after the junction. In Fig. 1.5A, the energy levels of the insulated semiconductors are aligned and referred to vacuum, which allows visualization of the relative position of the bands and their spacing in each semiconductor. The Fermi levels of each material, E_F, are described in terms of their respective work functions, ϕ_{W1} and ϕ_{W2}. Material 1 is of the n-type, and material 2 is of the p-type. The Fermi level refers to the total chemical potential of the electrons. In Fig. 1.5B, the semiconductors are placed in contact (again, the contact is already established when the semiconductors are manufactured), and an abrupt interface is formed, where the electron affinities of each semiconductor create a step at the contact. In Fig. 1.5C, the system reaches steady state, with a single Fermi level at a certain temperature. It is important to observe that the Fermi levels of each material remain the same as they were before junction creation, considering their position relative to V (V_n and V_p) and their respective work functions. The existence of a single Fermi level for the system requires the creation of an electrostatic potential between $x = -d_1$ and $x = d_2$, and a deformation of the valence and conduction bands and the local vacuum level around the junction. The difference

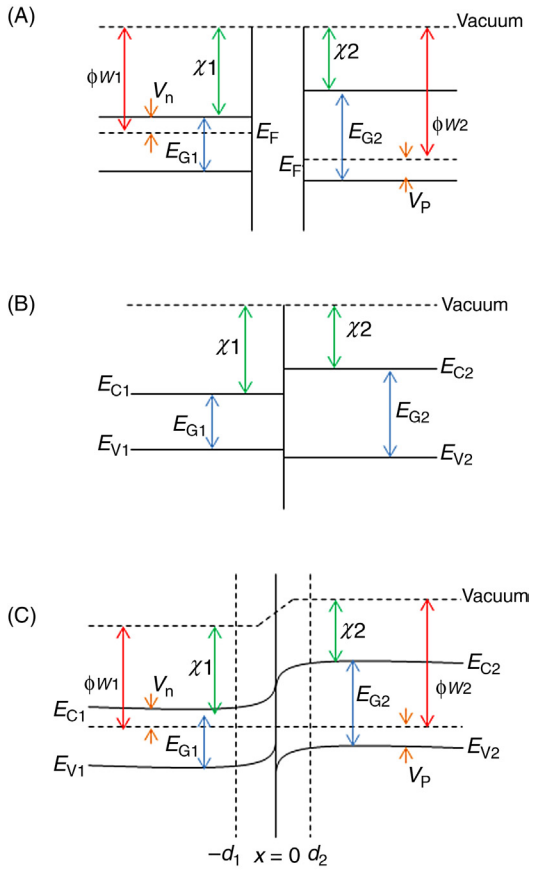

FIGURE 1.5 Electron energy levels of the n and p semiconductors. (A) Before contact, (B) during contact, and (C) after contact and in thermodynamic equilibrium. *Adapted from S.J. Fonash, Solar Cell Device Physics, second ed., Academic Press, Burlington, 2010 [16].*

of potential energy through the junction is the driving force to separate the charges generated after light absorption. The transport of the separated charges to the electrodes is performed efficiently by the absorbing film itself, which has high electron mobility [16].

In solar cells constructed from organic absorbers, such as dyes and conjugated polymers, or in cells sensitized with dyes or quantum dots, the absorption of light energy results in the formation of multiparticle excited species known as excitons [16]. An exciton is nothing more than an electron–gap pair, bonded by Coulombic attraction [18]. Therefore, they are species without charge that can move only by diffusion. The method of breaking exciton symmetry in these devices is to use donor–acceptor (D–A) architectures, in analogy to the p–n junction of traditional semiconductors [3]. The donor is the material that absorbs photons and generates excitons, and the acceptor is a material of high electron affinity. The difference in electron affinities between the donor and the acceptor results

in an electric potential large enough to cause the separation of charges at the interface of both materials [3]. However, the cell design must consider whether the separation of the D and A phases, as well as the thicknesses of the absorbing layer as a whole, is compatible with the lifetime and the diffusion length of the exciton. For example, the diffusion length of the excitons in most conjugated polymers used in OSCs is between 30 and 60 nm [3,16]. Therefore, the operation of organic or dye-sensitized cells depends decisively on the control of the morphology of the interfaces at the nanoscale. The following section presents details on the structure and operation of these types of cells.

1.2.3 Organic Solar Cells

OSCs use organic semiconductors, such as small organic dye or conjugated polymer molecules, in the absorber/donor function [19]. Coordination compounds, especially phthalocyanines and metalloporphyrins, can also be used in this function, although they are not organic substances, strictly speaking [3,19]. Fullerene is the most common acceptor, although other polymers and small conjugated molecules [19], carbon nanotubes [20], and metal oxide nanoparticles [21] can also be used in this function. Figs. 1.6 and 1.7 illustrate the structural formulas of the main absorbing materials and fullerenes used to build OSCs.

The first models of this type of cell were proposed in the 1980s, with organic pigments films placed between two metal electrodes with different work functions [22]. However, the efficiency of these cells was very low (<0.1%). Years later, the use of the D–A junction in the bilayer concept, employing other dyes, such as phthalocyanines, increased the conversion efficiency to almost 1% [23]. This figure was surpassed only at the beginning of the 2000s with the introduction of bulk heterojunction solar cells based on blends of conjugated polymers and fullerenes [24,25]. Today, the best conversion efficiencies are 12% for cells based on small molecules [12b] and 9.2% for cells based on conjugated polymers [26]. Efficiency values of 15% are expected in the near future [27,28]. In addition, there is consensus on the fact that efficiency has a secondary role in the dissemination of organic cells; the most important metric is the lower watt/hour cost of these devices. Fig. 1.6 shows the structures of absorbers used in OCSs along with the photovoltaic parameters of the respective cells fabricated under optimized conditions.

The field of OSCs gained force with the introduction of conjugated polymers as absorbing material. In addition to their optoelectronic properties, conjugated polymers can be processed in solution and at room temperature by the fast printing processes used in the printing and textile industries, such as roll-to-roll and screen printing [29]. Due to this versatility, the cell manufacturing cost is even lower. In addition, the polymer films can be deposited on plastic substrates, which allow the large-scale production of flexible cells (Fig. 1.8) and, consequently, their widespread use in buildings.

Conjugated polymers are formed by a main chain of sp^2 carbon atoms, with alternate single and double bonds. Due to conjugation, the electrons of the π bonds are dislocated by the polymer chain. As a result of the different lengths of the single and double bonds (single bonds are longer than double bonds), these materials exhibit a separation between

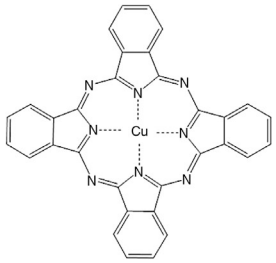

1
E_g: 3.1 eV
V_{OC}: 450 mV; J_{SC}: 2.3 mA.cm^{-2}
FF: 0.65; η: 0.95%

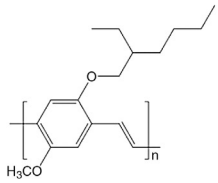

2
E_g: 2.3 eV
V_{OC}: 820 mV; J_{SC}: 5.3 mA.cm^{-2}
FF: 0.61; η: 2.5%

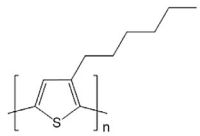

3
E_g: 2.0 eV
V_{OC}: 610 mV; J_{SC}: 11.1 mA.cm^{-2}
FF: 0.66; η: 5.0%

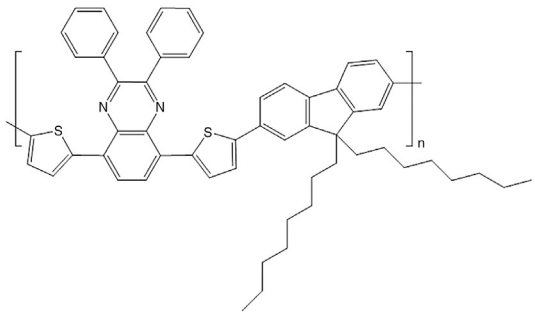

4
E_g: 1.9 eV
V_{OC}: 990 mV; J_{SC}: 9.7 mA.cm^{-2}
FF: 0.57; η: 5.5%

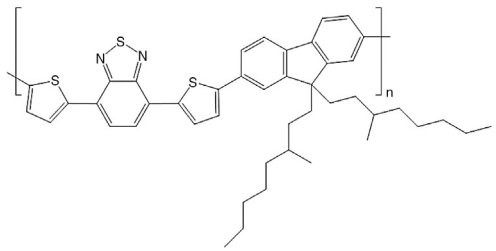

5
E_g: 1.9 eV
V_{OC}: 1000 mV; J_{SC}: 9.1 mA.cm^{-2}
FF: 0.51; η: 4.5%

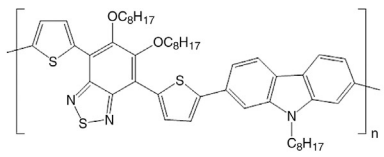

6
E_g: 1.9 eV
V_{OC}: 810 mV; J_{SC}: 9.6 mA.cm^{-2}
FF: 0.69; η: 5.4%

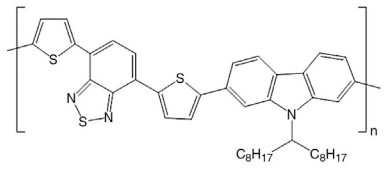

7
E_g: 1.8 eV
V_{OC}: 900 mV; J_{SC}: 12.1 mA.cm^{-2}
FF: 0.69; η: 6.8%

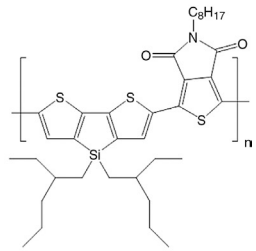

8
E_g: 1.8 eV
V_{OC}: 880 mV; J_{SC}: 12.2 mA.cm^{-2}
FF: 0.68; η: 7.3%

FIGURE 1.6 Structural formula of absorbing materials for organic solar cells (OCSs) and their respective photovoltaic parameters (for cells in optimized conditions). 1, Copper phthalocyanine; 2, MDMO-PPV; 3, P3HT; 4, NP7; 5, BisDMO-PFTDBT; 6, HXS-1; 7, PCDTBT; 8, PDTSPTBT.

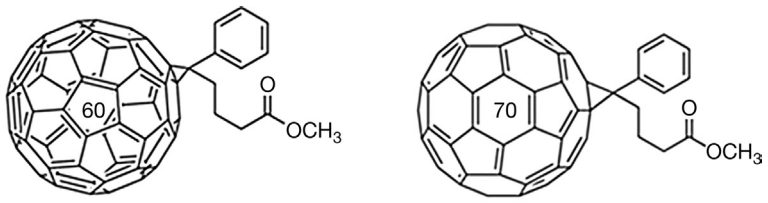

1 2

FIGURE 1.7 Structural formula of some fullerenes used in OSCs. 1, [6,6]-Phenyl-C61-butyric acid methyl ester (PC61BM); 2, [6,6]-phenyl-C71-butyric acid methyl ester (PC71BM).

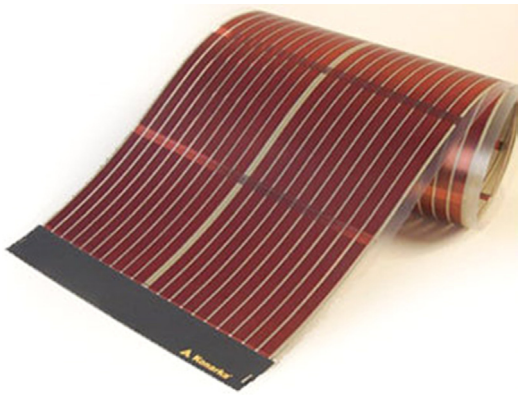

FIGURE 1.8 OCS module manufactured by Konarka. *From http://www.konarka.com/*

the valence and conduction bands that characterizes them as semiconductors [30]. Conduction at levels similar to those of metals is only possible when the polymer is doped [31]. In fact, most conjugated polymers have separation energies between bands above 2.0 eV (620 nm), which considerably limits solar light absorption. Another important feature is their electron mobility (for most conjugated polymers, it is lower than 0.01 $cm^2\ V^{-1}\ s^{-1}$), which is much lower than that of traditional semiconductors (e.g., the mobility of intrinsic silicon can be up to 10^4 times higher) [16]. By contrast, the optical absorption coefficient of these materials is extremely high, on the order of $10^5\ cm^{-1}$, so ultrathin films (thickness <100 nm) are sufficient to collect most of the incident photons and compensate for the low mobility [19].

The operation of OCSs is based essentially on the photoinduced electron transfer from the donor element to an acceptor of high electron affinity. Fig. 1.9 shows a schematic of the process, in which a conjugated polymer (donor) absorbs energy and injects the photoexcited electrons into the fullerene (acceptor) [32].

The process of electron transfer between dyes or conjugated polymers and fullerenes occurs on a much smaller time scale (on the order of femtoseconds) than that of

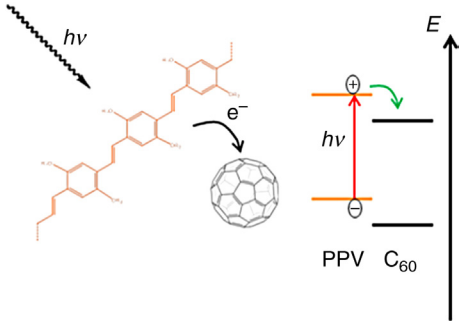

FIGURE 1.9 Schematics of the photoinduced electron transfer process from a *p*-phenylene-vinylene *(PPV)* molecule to a fullerene (C_{60}) and of the energy levels of each material. *Adapted from H. Hoppe, N.S. Sariciftci, Organic solar cells: an overview, J. Mater. Res. 19 (2004) 1924–1945 [19].*

competitive processes, such as photoluminescence (on the order of nanoseconds) [32,33]. The energy levels of the donor and the acceptor favor the vector transfer of the electrons. The junction region between the donor and the acceptor (D–A junction) of an OCS can be established in two ways, as illustrated in Fig. 1.10 [19]: (A) as a plane or bilayer heterojunction and (B) as a bulk heterojunction. In (A), a fullerene layer is deposited on the donor layer (small molecule or polymer) (Fig. 1.10A), and the heterojunction is established in the interface of the two layers, in the same way as in a p–n junction of an inorganic semiconductor. In Fig. 1.10B, the absorbing film is a blend of fullerene with a conjugated polymer, mixed throughout the entire volume of the film. The blend's morphology is developed on the nanoscale and provides a fundamental contribution to the photovoltaic conversion, as it significantly increases the interfacial area of the D–A junction [19].

The photovoltaic parameters of OSCs depend primarily on the energy levels of the electron donor and acceptor, as well as on the work function of the electrodes. The open-circuit voltage of an organic cell can be as high as the separation energy between the highest occupied molecular orbital (HOMO) of the donor and the lowest unoccupied molecular orbital (LUMO) of the acceptor [34]. Some studies indicate that in cells with conjugated polymers, the V_{oc} value has an inverse and linear relationship with the first reduction voltage (LUMO) of the fullerene compound (the lower the voltage is, the higher the V_{oc} of the corresponding cell) [34]. Likewise, there is a linear and direct relationship between the V_{oc} and the oxidation voltage (HOMO) of the polymer [34]. The interfaces of the absorbing layer with the electrodes also have an effect on the cell voltage. Tin oxide doped with indium (ITO) used as an anode has a work function of 4.7 eV, slightly lower than the HOMO levels of most dyes and conjugated polymers used in solar cells. To reduce the energy barrier in the electrode-active layer interface, this value can be increased by treating the ITO electrode with plasma or by depositing layers of conductive polymers of nanometric thickness, such as the poly(3,4-ethylenedioxytiophene)-poly(styrenesulfonic acid) (PEDOT:PSS) complex or the polyaniline (PANI) complex [35–37]. The cathode consists of a metal with a low work function, such as aluminum.

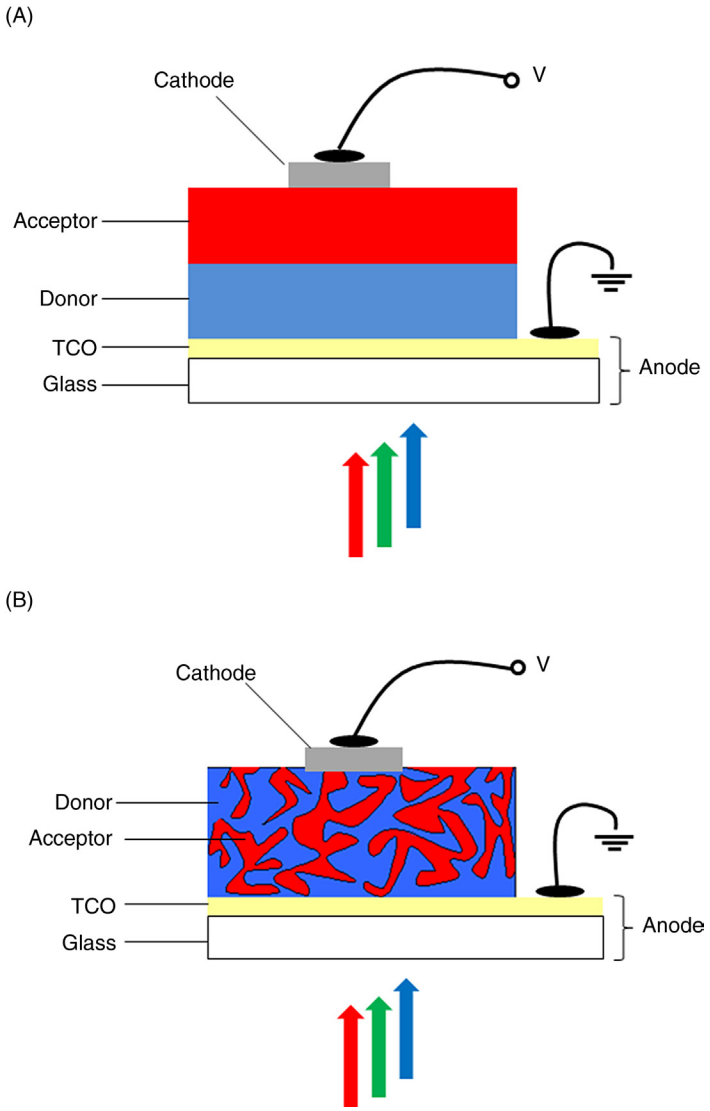

FIGURE 1.10 Schematic of an OSC for the bilayer heterojunction (A) and bulk heterojunction (B) configurations.

The current density generated by a solar cell corresponds to the number of charges collected by the electrodes, which, in the case of OSCs, is the product of three efficiencies: photon absorption (η_{abs}), exciton dissociation (η_{diss}), and the collection of carriers by the electrodes (η_{out}) [19]:

$$J_{sc} = \eta_{abs} \cdot \eta_{diss} \cdot \eta_{out} \tag{1.12}$$

The absorption efficiency depends on the absorption spectrum of the absorbent material and on optical effects, especially interference, inside the device [38]. As mentioned,

the absorption coefficient of conjugated polymers, as well as that of small conjugated molecules and coordination compounds, is quite high. The OSC architecture features a relatively thick glass substrate adjacent to a highly reflective metal electrode. This combination establishes interference conditions, both constructive and destructive, that may disrupt the coincidence between the maximum amplitude of the electrooptical field and the D–A interface and, consequently, reduce the photon collection efficiency [19,38].

The dissociation efficiency of the excitons depends decisively on the interface between donor and acceptor. In bulk heterojunction OSCs (Fig. 1.10B), the morphology developed at the nanoscale must be controlled in a way that the phase segregation is minimal and the D–A interface has a dimension compatible with the exciton diffusion length [19,39,40]. Films consisting of 1:4 (m/m) MDMO-PPV:C_{60} deposited by spin coating on an ITO substrate have different morphologies when toluene or chlorobenzene is used to prepare the deposition solutions. Toluene causes the formation of globules of varied sizes up to 200 nm, possibly clustered structures that make the film surface more irregular. When chlorobenzene is used, segregation occurs at a much smaller scale, on the order of 20 nm, and the film surface appears smoother. The consequence of morphology on conversion efficiency is immediate; the efficiency of OSCs prepared using chlorobenzene is 3 times higher than that of those made with toluene [39].

The charge collection efficiency depends on the path inside the active layer that is taken by the carriers. The mobility of the materials composing the active layer has a critical role in this process. Mobility is very low in most conjugated polymers because of their disordered nature in the solid state. In these systems, the conduction mechanism occurs mainly by hopping of highly localized charge carriers [41–44]. The carrier mobility can be explained by the Poole–Frenkel model, where mobility μ is proportional to the electric field E, according to Eq. 1.13 [19]:

$$\mu(E) = \mu_0 \exp\left(\gamma\sqrt{E}\right) \tag{1.13}$$

where μ_0 is the mobility at 0 K and γ is a preexponential factor; both depend on the temperature. The electric field inside the device must be strong enough to drive the carriers to the electrodes, which requires the difference between the work functions of the electrodes to be maximized and the thickness of the active layer to be minimized (generally to less than 100 nm).

The *FF* and the overall conversion efficiency of a solar cell depend, in addition to V_{oc} and J_{sc}, on the optimization of the series and parallel resistances of the device (Section 2.1). The deposition of conductive polymers on the transparent electrode, before the active layer, reduces the contact resistance and, consequently, the R_s value [37]. The deposition of a LiF layer on the active layer, preceding the deposition of the metal cathode, increases the carrier collection by the electrode, which also contributes to reducing R_s [45]. The carrier mobility and lifetime (τ) also influence *FF* and η. The larger the $\mu \times \tau$ product is, the higher the cell efficiency.

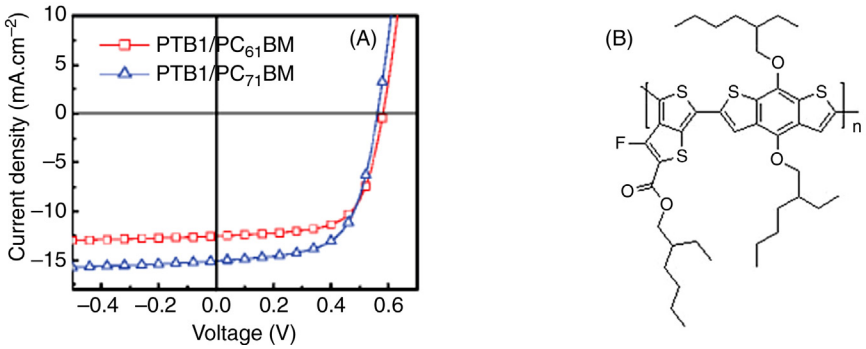

FIGURE 1.11 (A) $J \times V$ curves of OSCs subjected to AM1.5 irradiation (100 mW·cm^{-2}) prepared with two types of fullerenes as indicated, and (B) structural formula of the *PTB1* polymer used as an absorber/donor. *Reproduced with permission from Y. Liang, et al. Development of new semiconducting polymers for high performance solar cells, J. Am. Chem. Soc. 131 (2009) 56–57 [46].*

The most modern molecular engineering concept for the synthesis of conjugated polymers for OSCs is based on the preparation of monomers (and comonomers) with a modular structure. The modules are formed by a sequence of electron donating and accepting units (push–pull systems) that together with the main conjugated chain form chromophores with an absorption spectrum displaced to the red region (500–800 nm), a region with a more intense solar flux of photons [27]. Structures 4–8 illustrated in Fig. 1.6 are examples of this type of polymer. With this approach, the conversion efficiencies of the respective OSCs have reached the highest values of approximately 9.2% [27]. Fig. 1.11 shows the photovoltaic curves of OSCs that reached this efficiency record (9.2%) based on fullerenes and on the polymer absorber also shown in the figure [46].

1.2.4 Dye-Sensitized Solar Cells

The development of DSSCs began in the mid-1980s. A study revealed that colloidal TiO_2 particles (20 nm in diameter) could be sensitized to visible light by a ruthenium-based luminescent complex (tris(2,2′-bipyridine-4,4′-dicarboxylate) chloride of ruthenium(II)) [47]. In addition, the study found that the photoluminescence of the complex was completely extinguished when the complex was immobilized on the oxide nanoparticle, and thus, it was concluded that the complex transferred photoexcited electrons to the conduction band of the semiconductor. Years later, this principle was applied to a device, and the DSSC field has grown significantly since then [48]. Today, the overall conversion efficiency of these cells is higher than 11% [49,50].

A typical DSSC consists of a photoanode, a counter-electrode, and an electrolyte that separates the electrodes. The photoanode is constructed from a mesoporous and nanocrystalline film of a semiconductor with wide separation between bands, such as TiO_2, ZnO, or SnO_2, which is deposited on a transparent electrode, usually fluorine-doped tin oxide (FTO). The semiconductor is photosensitized by a dye, which may be a ruthenium(II) complex [51], quantum dots (CdSe, PbS) [52], synthetic organic dyes [53,54], or natural extracts [55,56]. Fig. 1.12 illustrates the structural formulas of the main dyes used in DSSCs.

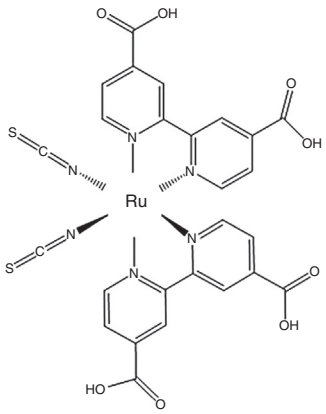

11
V_{OC}: 720 mV; J_{SC}: 18.2 mA.cm^{-2}
FF: 0.73; η: 10.0%

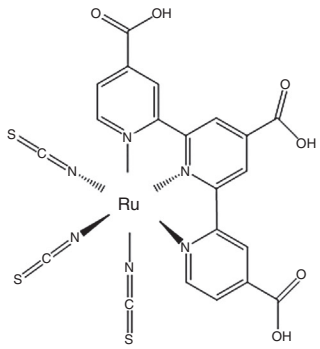

12
V_{OC}: 736 mV; J_{SC}: 20.9 mA.cm^{-2}
FF: 0.72; η: 11.1%

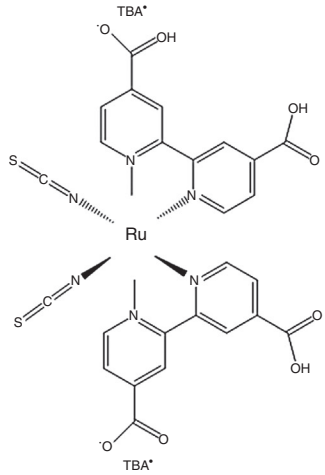

13
V_{OC}: 826 mV; J_{SC}: 17.0 mA.cm^{-2}
FF: 0.72; η: 10.1%

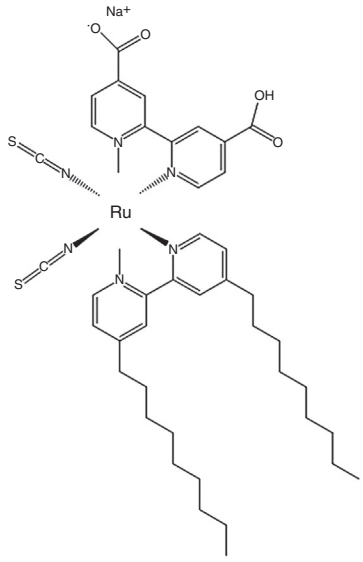

14
V_{OC}: 700 mV; J_{SC}: 15.9 mA.cm^{-2}
FF: 0.68; η: 7.2%

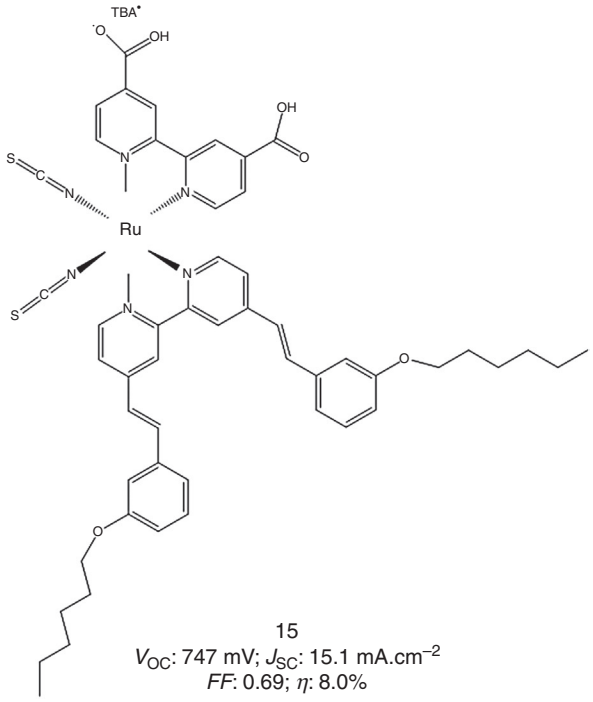

15
V_{OC}: 747 mV; J_{SC}: 15.1 mA.cm^{-2}
FF: 0.69; η: 8.0%

FIGURE 1.12 Structural formula of the main dyes used in dye-sensitized solar cells (DSSCs) and their respective photovoltaic parameters (for cells in optimized conditions). 11, N3; 12, N749; 13, N719; 14, Z907; 15, K19; 16, YD2-o-C8; 17, D205; 18, blackberry anthocyanin.

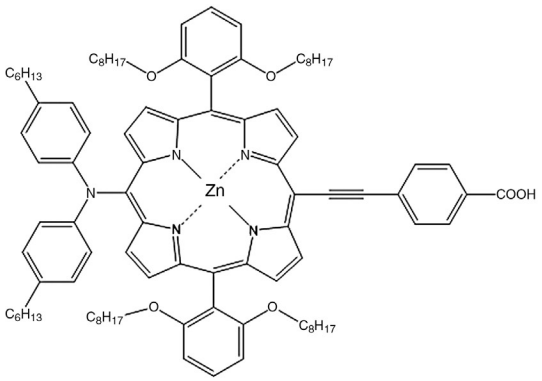

16
V_{OC}: 965 mV; J_{SC}: 17.3 mA.cm^{-2}
FF: 0.71; η: 11.9%

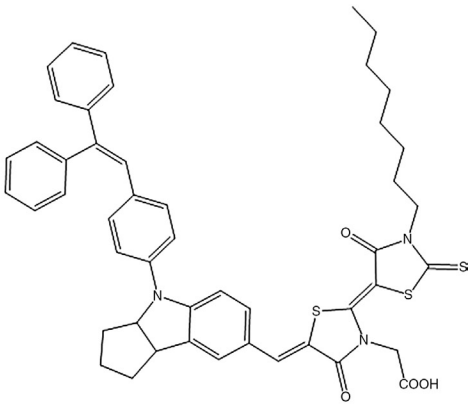

17
V_{OC}: 728 mV; J_{SC}: 13.7 mA.cm^{-2}
FF: 0.72; η: 7.2%

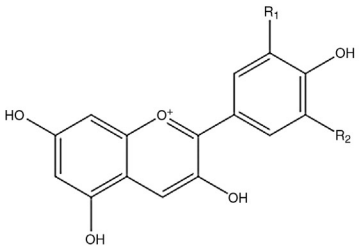

18
V_{OC}: 348 mV; J_{SC}: 15.1 mA.cm^{-2}
FF: 0.43; η: 1.15%

FIGURE 1.12 (*cont.*)

The electrolyte consists of a redox pair, such as I^-/I_3^-, cobalt(II/III) complexes, or TEMPO/TEMPO$^+$ (2,2,6,6-tetramethyl-1-piperidinyloxy) [51]. There is also the option of using ionic liquids [57,58], polymer electrolytes [59], and p-type semiconductors, including conjugated polymers [60,61]. The counter-electrode is formed by a transparent FTO electrode modified with a thin platinum layer. Some alternative materials can also be used, such as graphite and conductive polymers [62]. The operating principle of a DSSC and the morphology of the photoanode are schematized in Fig. 1.13A and 1.13B, respectively.

According to Fig. 1.13A, the photoexcited dye (S*) injects electrons into the semiconductor's conduction band. The photoinjected electrons are then collected by the transparent electrode to generate an anodic current in the circuit external to the cell. The photoexcited dye receives electrons from the electrolyte's redox pair and is then regenerated to its ground state. The redox pair is in turn regenerated by the electrons from the external circuit that are captured by the counter-electrode. An equivalent process occurs when the redox pair is replaced by organic semiconductors [61]. The cell operates in a cyclic and regenerative way, without any permanent chemical transformation. Differently from OSCs, in DSSCs, the energy absorption and charge transport are performed by different

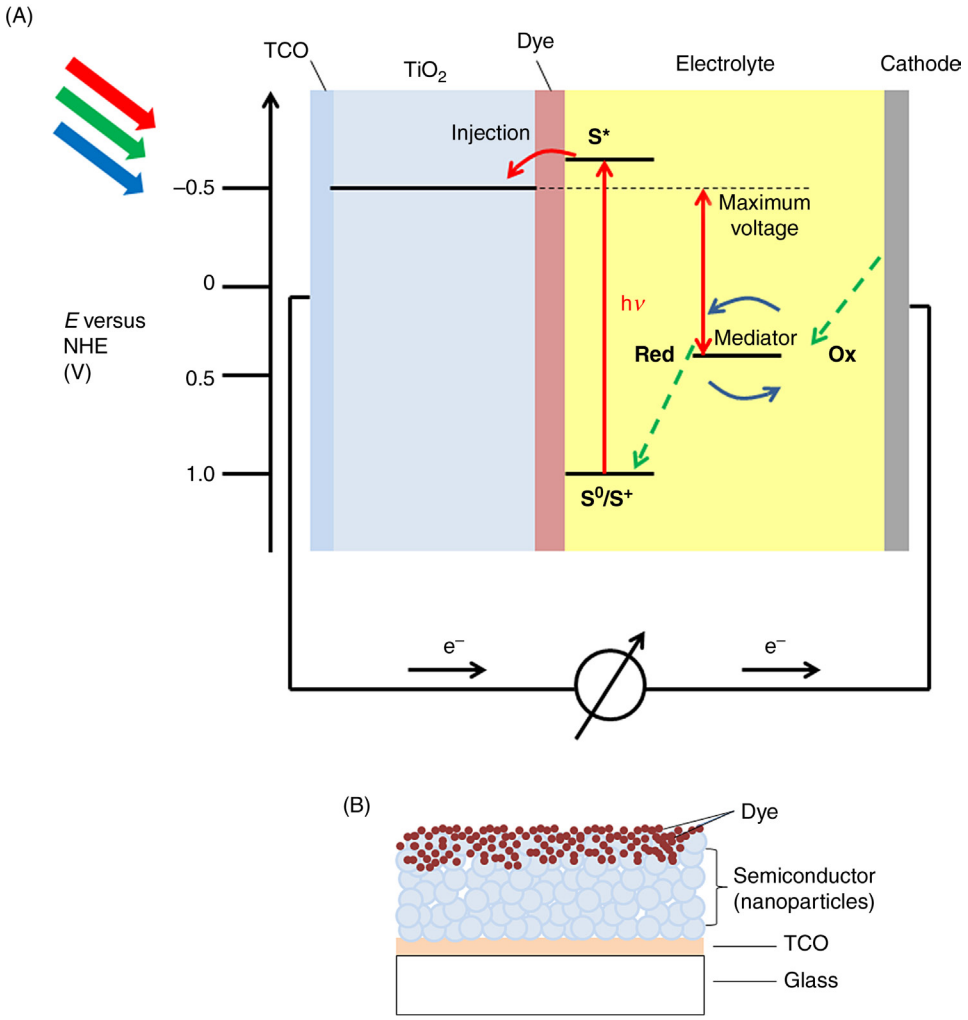

FIGURE 1.13 Schematics of a DSSC. (A) Side view of the DSSC indicating the oxidation–reduction voltages of the dye and mediator, and the position of the semiconductor's conduction band relative to the normal hydrogen electrode *(NHE)*. (B) Amplified side view of the photoanode with emphasis on the semiconductor nanoparticles sensitized with dye molecules. *Adapted from M. Gratzel, Recent advances in sensitized mesoscopic solar cells, Acc. Chem. Res. 42 (2009) 1788–1798 [51].*

elements in the device, a feature that widens the options of different absorbing materials and electrodes.

The efficiency of light conversion into electricity by DSSCs depends on effective electron coupling between the excited state of the photosensitizer and the semiconductor's conduction band. This condition is met mainly by the combination of ruthenium(II)-based dyes and TiO_2 mesoporous films, which has the highest conversion values [63,64]. The polypyridine complexes of ruthenium(II) (structures 11–15, Fig. 1.12) strongly absorb

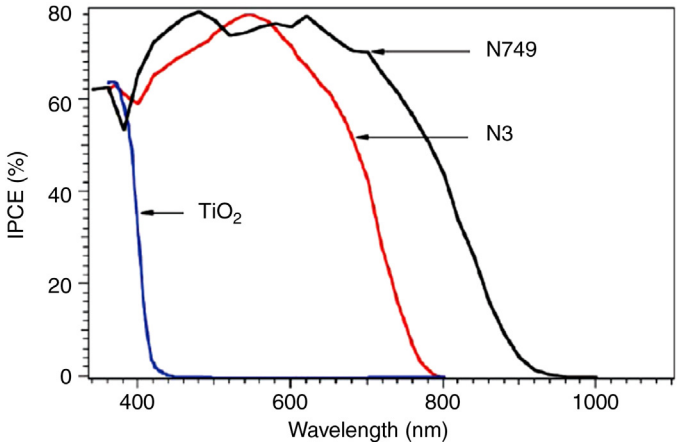

FIGURE 1.14 Incident photon to current efficiency *(IPCE)* curves of photosensitizers based on ruthenium(II) complexes (N3, N749) and pure TiO_2 mesoporous films. The chemical structure of the photosensitizers is shown next to the curves. *Reproduced with permission from M. Gratzel, Recent advances in sensitized mesoscopic solar cells, Acc. Chem. Res. 42 (2009) 1788–1798 [51].*

visible light because of the metal-to-ligand charge transfer (MLCT) type of transition [65,66]. In addition to the intense absorption, the energy levels of these complexes favor the electron transfer to the semiconductor, which occurs in nanoseconds to femtoseconds and, similar to OSCs, is much faster than recombination processes.

The voltage produced by an illuminated DSSC corresponds to the difference between the Fermi level of the electrons on the TiO_2 nanoparticles and the redox potential of the electrolyte (in DSSCs with semiconductors instead of a redox pair, this voltage is the chemical potential of the gaps) [51]. For a large number of photosensitizers anchored on TiO_2 nanoparticles, the driving force for electron injection is 0.15 eV [67]. However, the energy consumed to regenerate the photosensitizer is 0.6 eV. This imbalance is minimized by photosensitizers that have a redox potential closer to the redox potential of the iodide/triiodide pair (or another mediator). Another strategy to increase the efficiency of DSSCs is to extend the absorption range of the dye to the infrared region. The EQE of DSSCs based on two ruthenium(II) complex photosensitizers (N3 and N749) is as high as 80%, as shown in Fig. 1.14 [51]. Moreover, the spectral response of photosensitizer N749 extends to the near infrared, so an even wider range of the solar spectrum can be used by the cell. Therefore, the conversion efficiency increases 1.5-fold compared to the cell prepared with N3. As shown in Fig. 1.13, the photoelectrochemical parameters of current DSSCs are very promising; values of J_{sc} on the order of 20 mA cm^2, V_{oc} between 0.7 and 0.86 V, and *FF* between 0.65 and 0.8 have been found for cells under AM1.5 solar irradiation.

Ruthenium complexes are the main photosensitizers used in DSSCs. However, porphyrin-based DSSCs (structure 16, Fig. 1.12) have conversion efficiencies on the order of 12% [68]. Metal-free dyes are synthesized or extracted from natural sources to be used as photosensitizers. Synthetic organic dyes to be used in DSSCs must have electron donating and electron conducting units and anchoring groups (structure 17, Fig. 1.12) [69–72]. Natural

extracts of berries, such as blackberry, raspberry, and açaí, are rich in anthocyanins, which are flavonoids that inhibit the action of free radicals and can be used as photosensitizers in DSSCs [73]. The anthocyanin molecule (structure 18, Fig. 1.12) has hydroxyl groups that can anchor to the TiO_2 surface and, when photoexcited, is able to inject electrons in the semiconductor's conduction band. The stability of a DSSC sensitized with blackberry extract was evaluated, and it was concluded that it is comparable to that of a DSSC sensitized with N3 as long as the device is adequately sealed [74].

The mesoporous and nanocrystalline layer of a semiconductor oxide (Fig. 1.13B) and the photosensitizer are key elements of the DSSC. The nanoparticles are usually produced by the sol–gel method, followed by hydrothermal growth up to a size of 20–25 nm [75]. Once obtained, the nanoparticles are dispersed in a paste prepared with a stabilizing agent, such as poly(ethylene oxide). The paste is spread on the surface of the transparent electrode, which is then placed in an oven for sintering. The sintering process creates a connection between the particles that ensures electrical contact throughout the entire mesoscopic structure. The pores' mesoscopic structure significantly increases the surface area of the semiconductor film, which increases the amount of photosensitizer absorbed. Consequently, the light absorption capacity of the mesoporous system is much higher than that of a compact film. TiO_2 in anatase form is the most widely used semiconductor in DSSCs. The TiO_2 particles in this form have a bipyramidal shape, with facets exposed to the (101) direction, which is the direction with the lowest surface energy [51]. Fig. 1.15 shows the morphology of a TiO_2 mesoporous film used in DSSCs. In general, the thickness of a

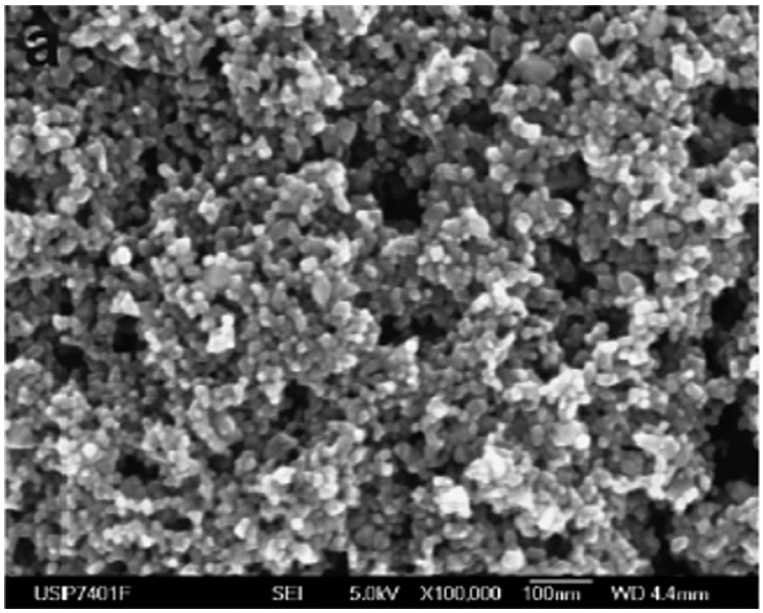

FIGURE 1.15 Scanning electron microscopy micrograph of a TiO_2 mesoporous film. *Reproduced with permission from A.O.T. Patrocinio, et al., Layer-by-layer TiO_2 films as efficient blocking layers in dye-sensitized solar cells, J. Photochem. Photobiol. A 205 (2009) 23–27 [78].*

semiconductor's mesoporous layer is 5–10 μm. In the dark, this semiconductor is an insulator because the separation energy between the bands is very high (3.2 eV). However, when electrons are injected into a TiO_2 nanoparticle during DSSC operation, the electron concentration can increase to up to 10^{17} cm^3, corresponding to a conductivity of 10^{-4} S cm^{-1} [67]. The charge transport mechanism inside the material is still not entirely understood. Nevertheless, there is consensus that the photoinjected electrons are caught in traps in the semiconductor, and once these traps are filled, the electrons begin to move freely by diffusion. The electron diffusion coefficient is not fixed but rather increases with light intensity. In addition, electron transport is accompanied by the movement of cations in the electrolyte, whose role is to avoid the formation of a noncompensated spatial charge that would certainly hinder the movement of electrons through the semiconductor [67]. The mesoporous film also has a terminal layer (∼5 μm) of larger particles (400–500 nm) used to increase the optical path and the light collection in the red region [67].

In addition to the photosensitizer dye and the semiconductor film, a DSSC is composed of other parts: the electrolyte and the counter-electrode. The electrolyte has a support role in the operation of the DSSC and is responsible for the regeneration of the photosensitizer to its ground state. Depending on the aggregation state of the electrolyte, it can be classified as a liquid, solid, or gel [61]. A liquid electrolyte is usually prepared with a redox pair, such as iodide/triiodide, dissolved in acetonitrile. In many cases, a solvent mixture is prepared to facilitate dispersion through the mesoporous layer and to passivate empty sites on the semiconductor surface. From a technological point of view, two important issues related to the use of liquid electrolytes must be considered. First, the photosensitizer's regeneration by the redox pair occurs mainly by diffusion, which is more effective when the electrolyte is less viscous. Second, the use of a liquid solvent requires effective sealing of the device to avoid solvent leakage and evaporation. Some alternatives have been proposed and tested, such as solid and gel polymer electrolytes, such as poly(ethylene oxide) impregnated with iodide/triiodide, organic conductors, such as PEDOT:PSS and spiro-OMeTAD, or even mixtures of a liquid solvent with an ionic liquid. Ionic liquids are being investigated as candidates for the partial or total substitution of organic solvent-based electrolytes in DSSCs [58]. The low vapor pressure of ionic liquids is ideal for outdoor applications, such as solar panels in buildings. However, the diffusivity of the redox pair in ionic liquids is low, which requires studies to optimize the electrolyte composition. In addition, there is one photosensitizer better adapted to each type of mediator system or electrolyte, which makes the choice of the mediator even less straightforward.

The DSSC performance is significantly reduced by recombination reactions [76]. In the case of liquid electrolyte DSSCs, the reaction between the photoinjected electrons and I_3^- occurs preferably at the FTO/semiconductor interface because of the permanent contact of the electrolyte with the conductive electrode. However, this reaction can be inhibited by a compact layer placed between the electrode and the semiconductor layer that physically blocks the contact of the I_3^- ions of the electrolyte with the photoinjected electrons in the electrode [77]. This layer is usually made of the same semiconductor used in the

mesoporous layer, although it is thinner, on the order of 100–200 nm. The self-assembly technique seems to be a promising method for deposition of the blocking layer because of its high degree of control of the film's thickness and morphology at the nanoscale and its low execution cost [78,79]. Basically, the technique consists of the successive and alternate immersion of a solid substrate in suspensions of anionic and cationic materials. This procedure results in the spontaneous adsorption of ultrathin layers, whose thicknesses are regulated by the conditions of the suspensions (i.e., concentration, pH, and ionic strength) [80]. Blocking layers composed of TiO_2 cationic particles (5 nm in diameter) and the polyanion poly(styrene sulfonic acid) PSS on FTO electrodes formed prior to the deposition of the TiO_2 mesoporous layer increased the overall conversion efficiency of an N3-based DSSC by 30% [78]. In addition, it was confirmed that the self-assembled layer not only blocks recombination but also improves the electrical contact between the electrode and the mesoporous layer, and both effects are responsible for the improvement in cell performance [81].

1.3 Photoelectrochemical Cells for the Production of Solar Fuels

Solar cells are devices that convert solar energy directly into electricity; therefore, they represent a feasible alternative to produce clean and cheap energy. However, one might ask how to produce energy at night? The Sun is an intermittent energy source, and it is estimated that only 6 h of the total solar irradiation are available for conversion to other useful forms of energy. Therefore, for solar energy to be a primary energy source, it must be associated with effective means of storage. To address this issue, we look at nature and how approaches have emerged naturally to produce and store energy from the Sun. The answer is photosynthesis. Briefly, photosynthesis can be described as the process through which plants absorb and convert solar energy, together with CO_2 and H_2O, into chemical energy in the form of substances with high energy content, such as carbohydrates [82]. Far from being science fiction, actual ways to artificially reproduce photosynthesis are being researched today. This strategy would allow the conversion of solar energy into high-energy products that could be used as fuel in power plants or to generate electricity in fuel cells during the night or at any time of the day.

Direct conversion of solar light into fuels (solar fuels) consists of transforming solar energy into energy stored in chemical bonds with the aid of a photocatalyst [14]. Solar fuels are an attractive solution toward energy sustainability because they can store large amounts of energy for a virtually unlimited time. The two most researched artificial photosynthesis techniques are based on the water-splitting reaction to produce molecular hydrogen (reaction 1.I) and the CO_2 reduction reaction to produce methanol or hydrocarbons (reaction 1.II):

$$2H_2O + 4h\nu \rightarrow 2H_2 + O_2 \ (\Delta G^o = 4.92 \text{ eV}, n = 4) \tag{1.I}$$

$$2H_2O + CO_2 + 8h\nu \rightarrow CH_4 + 2O_2 \ (\Delta G^o = 10.3 \text{ eV}, n = 8) \quad (1.II)$$

where n is the number of transferred electrons. Both reactions are thermodynamically unfavorable and involve a large number of transferred electrons. Thus, it is necessary to develop a photocatalytic system able to provide the electrochemical potential required to drive the reactions and allow efficient conversion of solar energy into chemical energy. Although water electrolysis is a well-established technology, it depends on the use of platinum as an electrocatalyst to accelerate the hydrogen evolution and water oxidation reactions. Platinum is a noble and expensive metal that does not represent a sustainable source. Therefore, it is necessary to develop lower cost photocatalytic systems that can be produced from sustainable sources.

A photoelectrochemical cell for artificial photosynthesis consists essentially of a pair of electrodes, with one or both made of a photoactive material, and an electrolyte responsible for completing the path between the electrodes and the external circuit [14]. The electrode made of the photoactive material acts as a photocatalyst; that is, it absorbs and converts solar energy at the oxidation–reduction potentials necessary to perform the water splitting or CO_2 reduction reactions. Different semiconductor materials can be used as photocatalysts in the water splitting reaction, as illustrated in Fig. 1.16. Hematite (α-Fe_2O_3) in particular is very promising. Its theoretical light-into-hydrogen conversion efficiency is 16.8% [83]. Pure TiO_2 is an excellent photocatalyst when excited with UV light [84], but it must be dye-photosensitized for the visible and infrared ranges. Photocatalytic systems based on metal complexes [85–87] and biocatalysts [88,89] (enzymes, especially hydrogenases and dehydrogenases) have also been tested for both water splitting and CO_2 reduction. Noble metals and their oxides (e.g., Pt, Pd, RuO_x, and IrO_x) are generally used as cocatalysts to accelerate the O_2 and H_2 evolution reactions. However, high cost and low abundance limit the large-scale production of photoelectrochemical cells with this type of electrocatalyst [14].

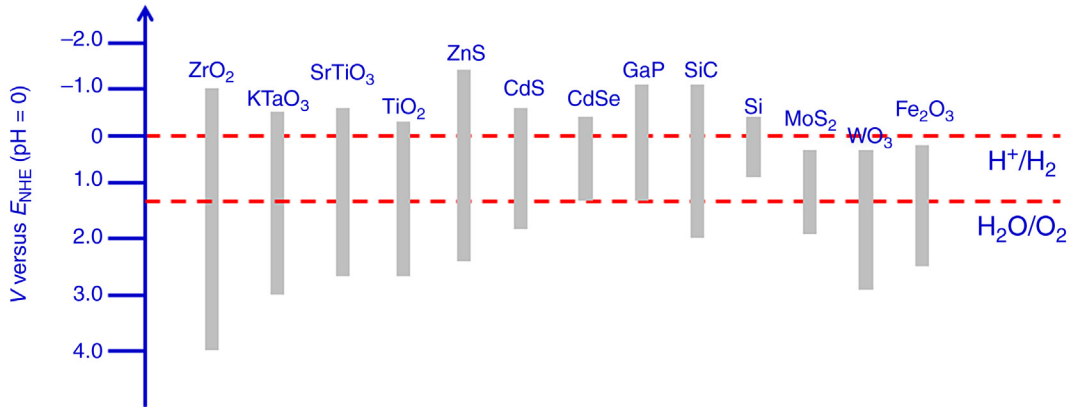

FIGURE 1.16 Energy levels of inorganic semiconductors in aqueous medium of pH 0. The *horizontal dashed lines* in *red* represent the oxidation potential of water (1.23 V) and the reduction potential of the proton (0 V). *Adapted from P.D. Tran, et al., Recent advances in hybrid photocatalysts for solar fuel production, Energy Environ. Sci. 5 (2012) 5902–5918 [14].*

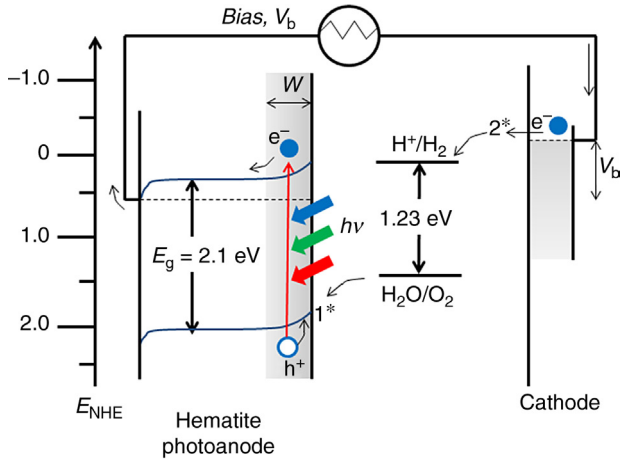

1^*: $2OH^- + 2h^+ \quad H_2O + ½\ O_2$

2^*: $2H_2O + 2e^- \quad H_2 + 2OH^-$

FIGURE 1.17 Schematic of a photoelectrochemical cell for water oxidation based on a hematite photoanode. The energy levels of the semiconductor and the water oxidation and H^+ reduction reactions are indicated in relation to the potential of the NHE. *Adapted from K. Sivula, et al., Solar water splitting: progress using alfa-Fe_2O_3 photoelectrodes, ChemSusChem 4 (2011) 432–449 [83].*

One of the most researched photoelectrochemical cell prototypes for the production of hydrogen from water photodecomposition uses photoanodes manufactured with hematite nanostructured films [83]. Hematite is the most stable crystalline form of iron oxide. It exhibits semiconductor behavior with a band separation energy of 2.1 eV, is stable at operating conditions, and is available cheaply. A schematic of a hematite-based photoelectrochemical cell and its operating principle during water photooxidation is shown in Fig. 1.17. The energy levels of hematite's valence and conduction bands, the water oxidation potential, and the proton reduction potential are also represented. When light is absorbed, the electrons are promoted to hematite's conduction band and the remaining gaps in the valence band are used in the O_2 evolution reaction (reaction 1.I). In the second stage, the electrons in the photoanode's conduction band are transferred to the external circuit until reaching the cathode, where they reduce protons to generate H_2 (reaction 1.II). The electrolyte medium may be an aqueous solution of a base, such as a sodium hydroxide solution of pH ~ 13.

As shown in Fig. 1.18, the level of the hematite conduction band is not sufficient to reduce the proton to hydrogen. This requires the application of an overvoltage in the cell for photooxidation to begin. The overvoltage can be supplied by a photovoltaic cell connected in series to the photooxidation cell [83]. Hematite has other limitations that must be considered: a low absorption coefficient that requires thick films (400–500 nm) for full light absorption, low conductivity of the major carriers, and a

very short diffusion length (L_d = 2–4 nm) of the minor carriers. Nanotechnology has been applied to overcome these limitations to produce hematite photoanodes with ideal performance. The overvoltage (up to 1.0 V) required to begin the water splitting process with hematite photoanodes is due to surface effects of the material. First, the presence of oxygen vacancies and the crystalline disorder create electron states in the middle of the forbidden band that act as traps for the gaps. In addition, the oxygen evolution reaction promoted by the hematite is very slow. The application of a passivating layer, such as Al_2O_3, and a layer of cobalt(II) or amorphous cobalt(II) phosphate eliminates the surface states and catalyzes the oxygen evolution reaction, respectively, to reduce overvoltage to close to 0.1–0.3 V [83]. The control of the morphology and the use of dopants such as Si significantly improve light absorption and the electrode's conductivity. Hematite films doped with Si and of columnar morphology, with "cauliflower-shaped" nanostructured columns, currently have the highest conversion efficiencies of solar light into hydrogen (2.1%) [90]. Fig. 1.19 shows a micrograph and the photoelectrochemical response of a hematite photoanode with this morphology.

Fig. 1.18B shows that at 1.23 V (water oxidation potential), the photocurrent density is 2.3 mA cm^{-2}, the highest value achieved to date [90]. The functionalization of the electrode's surface with cobalt ($Co(OH)_2$) increases the photocurrent to 2.7 mA cm^{-2} and alters the initiation of photooxidation by approximately 80 mV. Other studies have also demonstrated that nanostructured films of pure hematite are potentially promising as long as the growth of the columnar nanostructures has a preferential crystallographic orientation, under which charge transport is more effective [91]. Thus, it is believed that the development of nanotechnology will result in new methods to increase the conversion efficiency of hematite-based cells.

Coordination compounds based on ruthenium, cobalt, and nickel can be used to sensitize semiconductor electrodes and as cocatalysts of the O_2 evolution reaction. One of these complexes $[(4,4'\text{-}((HO)_2P(O)CH_2)_2bpy)_2Ru^{II}(bpm)Ru^{II}(Mebimpy)(OH_2)]^{4+}$, where bpy = 2,2′-bipyridine, bpm = 2,2′-bipyrazine, and Mebimpy = 2,6-bis(1-methylbenzimidazol-2-yl)pyridine), whose structure immobilized on an electrode is shown in Fig. 1.19, has different "modules" for each task, conceived to mimic the biological system of photosynthesis [87,92,93]. The group that is bonded directly to the electrode is the chromophore responsible for sensitization. Under the action of light, it injects electrons into the semiconductor, which are transferred to the external circuit up to the cathode. The more external group is the catalytic center that oxidizes the water molecules to O^{2+} and H^+. In addition, the electrons removed in this reaction are transferred to the chromophore part through a "bridge" (2,2′-bipyrazine unit). The electrons that reach the cathode are utilized in the reduction reaction, $2H^+ + 2e^- \rightarrow H_2$. Electrochemical studies show that the catalytic system is stable for up to 28,000 cycles without signs of deterioration [93]. However, under longer operation times and because of the environmental conditions, which are usually very oxidizing, the organic ligands of the complex degrade. These systems are

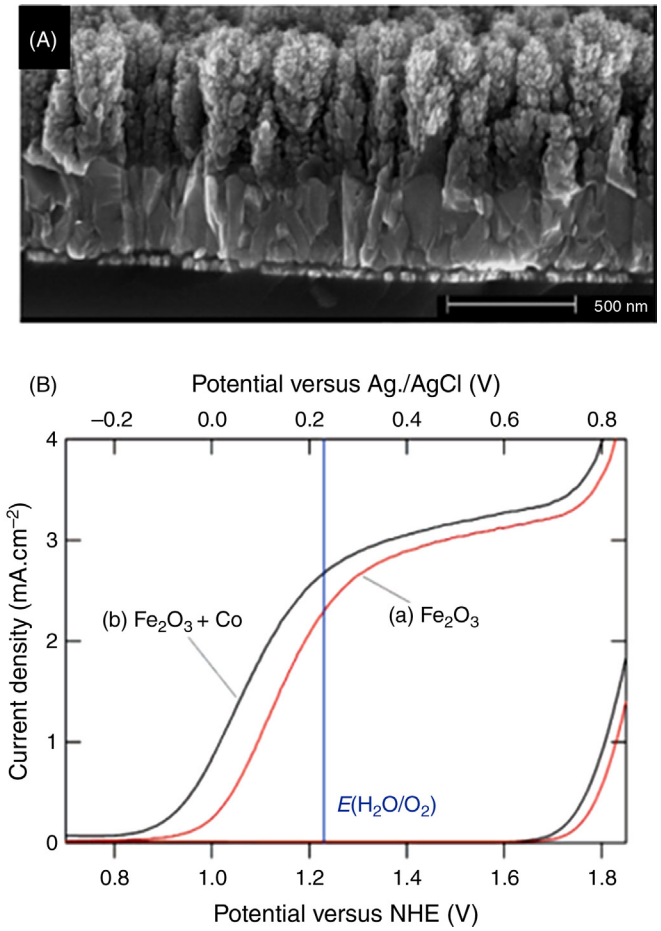

FIGURE 1.18 (A) Cross-section of a hematite film grown by chemical vapor deposition on an fluorine-doped tin oxide (FTO) substrate. (B) $J \times V$ curves of the hematite film in the dark and under simulated illumination (AM1.5) without modification and modified with cobalt, as indicated. *Reproduced with permission from A. Kay, et al., New benchmark for water photooxidation by nanostructured α-Fe2O3 films, J. Am. Chem. Soc. 128 (2006) 15714–15721 [90].*

not competitive for large-scale applications today, but they enable some of the photosynthesis reactions to be applied in a controlled manner.

Cobaloxime, a cobalt(III)-based complex, is another efficient catalyst of the H_2 evolution reaction, especially in strongly acidic media and organic solutions. The stability of this family of complexes is still low when immobilized on substrates to prepare photoelectrodes [14,85,86]. To date, only a few photoanodes based on cobalt complexes have been reported to enable the water splitting reaction. One potential candidate is based on an ITO electrode sensitized with perylene (an n-type organic semiconductor) and then covered with a second layer of cobalt phthalocyanine. When operated together with a platinum

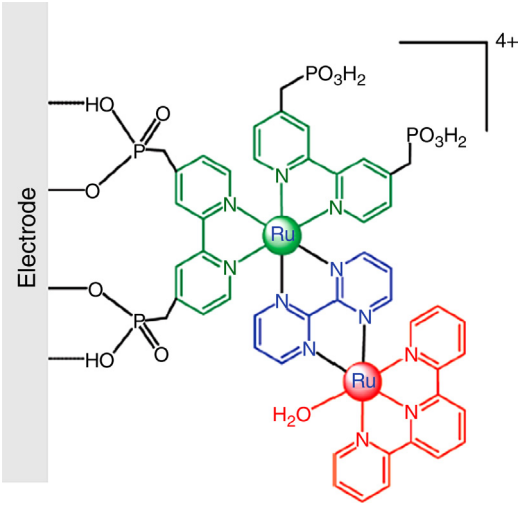

FIGURE 1.19 Structure of the complex $[(4,4'\text{-}((HO)_2P(O)CH_2)_2bpy)_2Ru^{II}(bpm)Ru^{II}(Mebimpy)(OH_2)]^{4+}$, where bpy = 2,2′-bipyridine, bpm = 2,2′-bipyrazine, and Mebimpy = 2,6-bis(1-methylbenzimidazol-2-yl)pyridine), immobilized on an electrode. *Reproduced with permission from J.J. Concepcion, et al., Making oxygen with ruthenium complexes, Acc. Chem. Res. 42 (2009) 1954–1965 [92].*

contraelectrode, this photoanode is able to split water (pH 11) in the presence of visible light under a voltage of 0.4 V (Ag/AgCl) and a yield of 3500 cycles/h [86].

1.4 Conclusions and Perspectives

Solar cells and photoelectrochemical cells for artificial photosynthesis are concrete solutions to current and future global energy demands and an alternative to the scarcity and environmental impact problems associated with fossil fuels. However, coordinated efforts among different segments of society—the scientific community, industry, and government—are still necessary to implement scientific discoveries and technological advances for the service of the population.

In terms of science and technology, conversion of solar light into useful energy is based on an established sequence of events—light absorption and charge transfer, separation and transport—that occur at very short times and at an atomic and molecular scale. Therefore, the role of nanotechnology is fundamental because nanomaterials can be used as construction blocks to assemble organized systems with virtually unlimited capabilities for solar light capture and charge transport. Thanks to a large number of semiconductors (both organic and inorganic) and new properties that manifest at the nanoscale, as well as the possibility for combination with molecular systems to increase light collection efficiency, third-generation solar cells (OSCs and DSSCs) are promising prospects to convert solar light into electricity. In addition, the possibility of having flexible (or even disposable) devices, fabricated with cheaper materials in much simpler manufacturing systems, is an

exclusive feature of these new cells. However, materials and devices with higher efficiency and stability still need to be developed for these cells to be effectively introduced into the market. The development of solar cells based on crystalline silicon was considered impractical in the past because of their high cost. However, the fact that silicon has ideal properties for photovoltaic conversion cannot be ignored, and silicon-based solar cells are now readily available. The same path must be followed in the case of third-generation solar cells.

Regarding artificial photosynthesis and the production of solar fuels, this field is still in an early development stage, but it looks very promising because of the discoveries with third-generation cells together with the consolidation of the photochemistry of coordination compounds and semiconductors. Although conversion efficiencies are still modest, the breakthroughs in cells based on hematite photoelectrodes are encouraging, especially considering that hematite is an abundant and low-cost material. The discoveries in the field of the photochemistry of coordination compounds go beyond energy production. Molecular photocatalytic systems have provided a single and elegant platform to study biological processes whose full understanding will certainly result in the development of more efficient energy conversion devices.

List of Symbols

DSSCs	Dye-sensitized solar cells
EQE	External quantum efficiency
FF	Fill factor
FTO	Fluorine-doped tin oxide
GHGs	Greenhouse gases
HOMO	Highest occupied molecular orbital
IPCE	Incident photon to current efficiency
ITO	Indium-doped tin oxide
$\mathbf{J_{sc}}$	Short-circuit current density
LUMO	Lowest occupied molecular orbital
MDMO-PPV	Poly[2-methoxy-5-(3′,7′-dimethyloctyloxy)-1,4-phenylenevinylene]
MLCT	Metal-to-ligand charge transfer
OSCs	Organic solar cells
PANI	Poly(aniline)
PC61BM	[6,6]-Phenyl-C61-butyric acid methyl ester
PC71BM	2, [6,6]-Phenyl-C71-butyric acid methyl ester
PEDOT:PSS	Poly(3,4-ethylenedioxytiophene)-poly(styrenesulfonic acid)
Pout	Power produced per illuminated area
PPV	Poly(p-phenylene vinylene)
PSS	Poly(styrenesulfonic acid)
spiro-OMeTAD	N2,N2,N2′,N2′,N7,N7,N7′,N7′-octakis(4-methoxyphenyl)-9,9′-spirobi[9H-fluorene]-2,2′,7,7′-tetramine
TCO	Transparent conductive oxide
TEMPO	2,2,6,6-Tetramethyl-1-piperidinyloxy
$\mathbf{V_{oc}}$	Open circuit voltage
η	Overall conversion efficiency

References

[1] N.S. Lewis, D.G. Nocera, Powering the planet: chemical challenges in solar energy utilization, Proc. Natl. Acad. Sci. USA 103 (2006) 15729–15735.

[2] M.E. Mann, et al., Global-scale temperature patterns and climate forcing over the past six centuries, Nature 392 (1998) 779–787.

[3] P.V. Kamat, Meeting the clean energy demand: nanostructure architectures for solar energy conversion, J. Phys. Chem. C 111 (2007) 2834–2860.

[4] http://www.institutocarbonobrasil.org.br

[5] Key World Energy Statistics, International World Agency, 2012.

[6] (a) http://en.wikipedia.org/wiki/Nuclear_power_in_the_United_States; (b) http://pt.wikipedia.org/wiki/Energia_nuclear_no_Japao

[7] http://pt.wikipedia.org/wiki/Acidente_nuclear_de_Chernobil

[8] http://pt.wikipedia.org/wiki/Acidente_nuclear_de_Fukushima_I

[9] M.S. Dresselhaus, I.L. Thomas, Alternative energy technologies, Nature 414 (2001) 332–337.

[10] N.S. Lewis, et al., Basic Energy Sciences Report on Basic Research Needs for Solar Energy Utilization, Office of Science, U.S. Department of Energy, Washington, DC, 2005, http://www.sc.doe.gov/bes/reports/files/SEU_rpt.pdf

[11] http://www.downtoearth.org.in/content/falling-silicon-prices-shakes-solar-manufacturing-industry

[12] (a) http://www.polyera.com; (b) http://www.heliatek.com; (c) http://www.plextronics.com; (d) http://www.solarmer.com; (e) http://www.konarka.com

[13] (a) http://www.g24i.com; (b) http://www.dyesol.com; (c) http://www.m-kagaku.co.jp; (d) http://www.solaronix.com

[14] P.D. Tran, et al., Recent advances in hybrid photocatalysts for solar fuel production, Energy Environ. Sci. 5 (2012) 5902–5918.

[15] http://org.ntnu.no/solarcells

[16] S.J. Fonash, Solar Cell Device Physics, second ed., Academic Press, Burlington, 2010.

[17] http://www.astm.org/standards

[18] C. Kittel, Introduction to Solid State Physics, eighth ed., John Wiley & Sons, New Jersey, 2005.

[19] H. Hoppe, N.S. Sariciftci, Organic solar cells: an overview, J. Mater. Res. 19 (2004) 1924–1945.

[20] A.F. Nogueira, et al., Polymer solar cells using single-wall carbon nanotubes modified with thiophene pendant groups, J. Phys. Chem. C 111 (2007) 18431–18438.

[21] S. Luzzati, et al., Photo-induced electron transfer from a dithienothiophene-based polymer to TiO_2, Thin Solid Films 403 (2002) 52–56.

[22] D. Wohrle, D. Meissner, Organic solar cells, Adv. Mater. 3 (1991) 129–138.

[23] C.W. Tang, Two-layer organic photovoltaic cell, Appl. Phys. Lett. 48 (1986) 183–185.

[24] G. Yu, et al., Polymerphotovoltaic cells: enhanced efficiencies via a network of internal donor-acceptor heterojunctions, Science 270 (1995) 1789–1791.

[25] C.Y. Yang, A.J. Heeger, Morphology of composites of semiconducting polymers mixed with C60, Synth. Met. 83 (1996) 85–88.

[26] Z. He, et al., Enhanced power conversion efficiency in polymer solar cells using an inverted device structure, Nat. Photon 6 (2012) 591–595.

[27] L. Bian, Recent progress in the design of narrow bandgap conjugated polymers for high efficiency organic solar cells, Prog. Polym. Sci. 37 (2012) 1292–1331.

[28] R.F. Service, Outlook brightens for plastic solar cells, Science 332 (2011) 293–303.

[29] F.C. Krebs, et al., Product integration of compact roll-to-roll processed polymer solar cell modules: methods and manufacture using flexographic printing, slot-die coating and rotary screen printing, J. Mater. Chem. 20 (2010) 8994–9001.

[30] A.J. Heeger, Nobel Lecture: semiconducting and metallic polymers: the fourth generation of polymeric materials, Rev. Mod. Phys. 73 (2001) 681–700.

[31] A.G. Macdiarmid, Synthetic metals: a novel role for organic polymers, Synth. Met. 125 (2001) 11–22.

[32] N.S. Sariciftci, et al., Photoinduced electron transfer from a conducting polymer to buckminsterfullerene, Science 258 (1992) 1474–1476.

[33] C.J. Brabec, et al., Tracing photoinduced electron transfer process in conjugated polymer/fullerene bulk heterojunctions in real time, Chem. Phys. Lett. 340 (2001) 232–236.

[34] M.C. Scharber, Design rules for donors in bulk-heterojunction solar cells—towards 10% energy-conversion efficiency, Adv. Mater. 18 (2006) 789–794.

[35] C.C. Wu, et al., Surface modification of indium tin oxide by plasma treatment: an effective method to improve the efficiency, brightness, and reliability of organic light-emitting devices, Appl. Phys. Lett. 70 (1997) 1348–1350.

[36] C. Ganzorig, M. Fujihira, Chemical modification of indium tin-oxide electrodes by surface molecular design, in: S.C. Moss (Ed.), Organic Optoelectronic Materials (Mater. Res. Soc. Symp. Proc. 708), Warrendale, PA, 2002, p. 83

[37] J.C.B. Santos, et al., Influence of polyaniline and phthalocyanine hole-transport layers on the electrical performance of light-emitting diodes using MEH-PPV as emissive material, Thin Solid Films 516 (2008) 3184–3188.

[38] L.A.A. Pettersson, et al., Modeling photocurrent action spectra of photovoltaic devices based on organic thin films, J. Appl. Phys. 86 (1999) 487–489.

[39] S.E. Shaheen, et al., 2.5% efficient organic plastic solar cells, Appl. Phys. Lett. 78 (2001) 841–843.

[40] H. Hoppe, et al., Nanoscale morphology of conjugated polymer/fullerene based bulk-heterojunction solar cells, Adv. Funct. Mater. 14 (2004) 1005–1011.

[41] P.W.M. Blom, et al., Electric-field and temperature dependence of the hole mobility in poly(*p*-phenylenevinylene), Phys. Rev. B 55 (1997) 656–659.

[42] L. Bozano, et al., Temperature- and field-dependent electron and hole mobilities in polymer light emitting diodes, Appl. Phys. Lett. 74 (1999) 1132–1134.

[43] V.D. Mihailetchi, et al., Electron transport in a methanofullerene, Adv. Funct. Mater. 13 (2003) 43–46.

[44] C. Melzer, et al., Hole transport in poly(phenylenevinylene)/methanofullerene bulk-heterojunction solar cells, Adv. Funct. Mater. 14 (2004) 865–870.

[45] C.J. Brabec, et al., Effect of LiF/metal electrodes on the performance of plastic solar cells, Appl. Phys. Lett. 80 (2002) 1288–1290.

[46] Y. Liang, et al., Development of new semiconducting polymers for high performance solar cells, J. Am. Chem. Soc. 131 (2009) 56–57.

[47] J. Desilvestro, et al., Highly efficient sensitization of titanium dioxide, J. Am. Chem. Soc. 107 (1985) 2988–2990.

[48] B. O'regan, M. Gratzel, A low-cost, high efficiency solar cell based on dye sensitized colloidal TiO_2 films, Nature 335 (1991) 737–740.

[49] Y. Chiba, et al., Dye sensitized solar cells with conversion efficiency of 11,1%, Jpn. J. Appl. Phys. Part 2 45 (2006) L638–640.

[50] J.M. Kroon, et al., Nanocrystalline dye sensitized solar cells having maximum performance, Prog. Photovolt. 15 (2007) 1–18.

[51] M. Gratzel, Recent advances in sensitized mesoscopic solar cells, Acc. Chem. Res. 42 (2009) 1788–1798.

[52] I. Robel, et al., Quantum dot solar cells: harvesting light energy with CdSe nanocrystals molecularly linked to mesoscopic TiO_2 films, J. Am. Chem. Soc. 128 (2006) 2385–2393.

[53] S. Ito, et al., High-conversion-efficiency organic dye-sensitized solar cells with a novel indoline dye, Chem. Commun. 10 (2008) 5194–5196.

[54] G. Zhang, et al., High efficiency and stable dye-sensitized solar cells with an organic chromophore featuring a binary π-conjugated spacer, Chem. Commun. 16 (2009) 2198–2200.

[55] A.S. Polo, N.Y.M. Iha, Blue sensitizers for solar cells: natural dyes from Calafate and Jaboticaba, Sol. Energy Mater. Sol. Cells 90 (2006) 1936–1944.

[56] A.O.T. Patrocinio, et al., Efficient and low cost devices for solar energy conversion: efficiency and stability of some natural-dye-sensitized solar cells, Synth. Met. 159 (2009) 2342–2344.

[57] M. Gratzel, Conversion of sunlight to electric power by nanocrystalline dye-sensitized solar cells, J. Photochem. Photobiol. A Chem. 164 (2004) 3–14.

[58] Y. Bai, et al., High-performance dye-sensitized solar cells based on solvent-free electrolytes produced from eutectic melts, Nat. Mater. 7 (2008) 626–630.

[59] A.F. Nogueira, et al., Dye-sensitized nanocrystalline solar cells employing a polymer electrolyte, Adv. Mater. 13 (2001) 826–830.

[60] Y. Saito, et al., Photo-sensitizing ruthenium complexes for solid state dye solar cells in combination with conducting polymers as hole conductors, Coord. Chem. Rev. 248 (2004) 1469–1478.

[61] B. Li, et al., Review of recent progress in solid-state dye-sensitized solar cells, Sol. Energy Mater. Sol. Cells 90 (2006) 549–573.

[62] T. Kitamura, et al., Improved solid-state dye solar cells with polypyrrole using a carbon-based counter electrode, Chem. Lett. 10 (2001) 1054–1055.

[63] A.S. Polo, et al., Metal complex sensitizers in dye-sensitized solar cells, Coord. Chem. Rev. 248 (2004) 1343–1361.

[64] R. Argazzi, et al., Design of molecular dyes for application in photoelectrochemical and eletrochromic devices based on nanocrystalline metal oxide semiconductors, Coord. Chem. Rev. 248 (2004) 1299–1316.

[65] J.P. Paris, W.W. Brandt, Charge transfer luminescence of a ruthenium(II) chelate, J. Am. Chem. Soc. 81 (1959) 5001–5002.

[66] K.W. Hipps, G.A. Crosby, Charge transfer excited states of ruthenium(II) complexes. III. Electron-ion coupling model for dπ* configurations, J. Am. Chem. Soc. 97 (1975) 7942–7948.

[67] M. Gratzel, Solar energy conversion by dye-sensitized photovoltaic cells, Inorg. Chem. 44 (2005) 6841–6851.

[68] A. Yella, et al., Porphyrin-sensitized solar cells with cobalt (II/III)–based redox electrolyte exceed 12 percent efficiency, Science 334 (2011) 629–633.

[69] K. Hara, et al., Novel conjugated organic dyes for efficient dye-sensitized solar cells, Adv. Funct. Mater. 15 (2005) 246–252.

[70] Z.S. Wang, Molecular design of coumarin dyes for stable and efficient organic dye-sensitized solar cells, J. Phys. Chem. C 112 (2008) 17011–17017.

[71] X.R. Song, D-π-A type organic photosensitizers with aromatic amine as electron-donating group—application in dye-sensitized solar cells, Prog. Chem. 20 (2008) 1524–1533.

[72] D. Kuang, Organic dye-sensitized ionic liquid based solar cells: remarkable enhancement in performance through molecular design of indoline sensitizers, Angew. Chem. Int. Ed. 47 (2008) 1923–1927.

[73] Q. Dai, J. Rabani, Photosensitization of nanocrystalline TiO_2 films by anthocyanin dyes, J. Photochem. Photobiol. A Chem. 148 (2002) 17–24.

[74] A.O.T. Patrocinio, N.Y.M. Iha, Em busca da sustentabilidade: células solares sensibilizadas por extratos naturais [Toward sustainability: solar cells sensitized by natural extracts], Quim. Nov. 33 (2010) 574–578.

[75] M.K. Nazeeruddin, et al., Conversion of light to electricity by Cis-X_2-bis(2,2'-bipyridyl-4,4'-dicarboxylate)ruthenium(II) charge transfer sensitizers (X = Cl^-, Br^-, I^-, CN^-, SCN^-) on nanocrystalline TiO_2 electrodes, J. Am. Chem. Soc. 115 (1993) 6382–6390.

[76] A.J. Frank, et al., Electrons in nanostructured TiO_2 solar cells: transport, recombination and photovoltaic properties, Coord. Chem. Rev. 248 (2004) 1165–1179.

[77] E. Palomares, et al., Control of charge recombination dynamics in dye sensitized solar cells by the use of conformally deposited metal oxide blocking layers, J. Am. Chem. Soc. 125 (2003) 475–482.

[78] A.O.T. Patrocinio, et al., Layer-by-layer TiO_2 films as efficient blocking layers in dye-sensitized solar cells, J. Photochem. Photobiol. A 205 (2009) 23–27.

[79] A.O.T. Patrocinio, et al., Filmes de óxidos semicondutores automontado [Self-assembled semiconductor oxide films], PI0802589-4 A2, deposit date 08/14/2008.

[80] L.G. Paterno, et al., Filmes poliméricos ultra-finos produzidos pela técnica de automontagem: preparação, propriedades e aplicações [Ultra-thin polymer films produced by the self-assembly technique: preparation, properties and applications], Quim. Nov. 24 (2001) 228–235.

[81] A.O.T. Patrocinio, et al., Role of polyelectrolyte for layer-by-layer compact TiO_2 films in efficiency enhanced dye-sensitized solar cells, J. Phys. Chem. C 114 (2010) 17954–17959.

[82] J. Whitmarsh, The photosynthetic process, in: G.S. Singhal, et al., (Ed.), Concepts in Photobiology: Photosynthesis and Photomorphogenesis, Kluwer Academic Publishers, Boston, 1999, pp. 11–51.

[83] K. Sivula, et al., Solar water splitting: progress using alfa-Fe_2O_3 photoelectrodes, ChemSusChem 4 (2011) 432–449.

[84] A. Fujishima, K. Honda, Electrochemical photolysis of water at a semiconductor electrode, Nature 238 (1972) 37–38.

[85] A.J. Esswein, D.G. Nocera, Hydrogen production by molecular photocatalysis, Chem. Rev. 107 (2007) 4022–4047.

[86] V. Artero, et al., Splitting water with cobalt, Angew. Chem. Int. Ed. 50 (2011) 7238–7266.

[87] J.J. Concepcion, et al., Chemical approaches to artificial photosynthesis, PNAS 109 (2012) 15560–15564.

[88] E. Reisner, et al., Visible light-driven H_2 production by hydrogenases attached to dye-sensitized TiO_2 nanoparticles, J. Am. Chem. Soc. 131 (2009) 18457–18466.

[89] T.W. Woolerton, et al., CO_2 photoreduction at enzyme-modified metal oxide nanoparticles, Energy Environ. Sci. 4 (2011) 2393–2399.

[90] A. Kay, et al., New benchmark for water photooxidation by nanostructured α-Fe_2O_3 films, J. Am. Chem. Soc. 128 (2006) 15714–15721.

[91] R.H. Gonçalves, et al., Magnetite colloidal nanocrystals: a facile pathway to prepare mesoporous hematite thin films for photoelectrochemical water splitting, J. Am. Chem. Soc. 133 (2011) 6012–6019.

[92] J.J. Concepcion, et al., Making oxygen with ruthenium complexes, Acc. Chem. Res. 42 (2009) 1954–1965.

[93] W. Song, et al., Making solar fuels by artificial photosynthesis, Pure Appl. Chem. 83 (2011) 749–768.